Int. J. Multiphase Flow, Vol. 4, pp. 535–551. Pergamon/Elsevier, 1978. Printed in Great Britain

MODELS FOR THE FORMATION OF GAS BUBBLES AT A SINGLE SUBMERGED ORIFICE IN A NON-NEWTONIAN FLUID

J. COSTES and C. ALRAN

Institut du Génie Chimique, Laboratoire Associé C.N.R.S. 192, Chemin de la loge, 31078 Toulouse Cedex, France

(*Received* 25 *July* 1977)

Abstract—Nitrogen bubbles were emitted by a single horizontal orifice submerged in an aqueous solution of sodium carboxymethylcellulose (C.M.C.). Their behaviour follows the Ostwald Dé Waele rheological model: $\tau = mE_0^n$; τ is the shear stress and E_0 the shear rate.

Experimental range of variables

Solution of C.M.C.					
% mass	m (kg.m^{-1} × s^{n-2})	n	ϕ (m)	$10^6 \times Q$ (m^3/s)	ΔP (Pa)
3	3.04	0.68	0.2530×10^{-2}	0–200	10–1500

Here, m and n are the parameters of the power law model, ϕ the orifice diameter, Q gas flow rate and ΔP the pressure drop at the orifice. Models of bubble formation in non-Newtonian liquids based on the concepts given by Davidson & Schuler (1960) and by Kumar & Kuloor (1969, 1970) have been developed under constant pressure and under constant flow rate conditions. When the Reynolds number at the orifice is lower than 1000, bubbles are formed under constant pressure conditions; for a Reynolds number greater than 1000, the bubbles are formed under constant flow rate conditions. The comparison of theoretical variation of bubble radius shows that Davidson & Schuler's and Kumar & Kudoor's models are in agreement, but Davidson & Schuler's models are more suitable to represent bubble formation.

1. INTRODUCTION

Bubbling gas in liquid is widely used in industrial processes, such as fluidized combustion of sulphur or hydrocarbons, ventilation of industrial liquid waste, polymerization reactions and fermentations where an intimate contact between viscous liquid and gas is not easily achieved.

As most industrial liquids are non-Newtonian, we have undertaken research on the formation and hydrodynamics of bubbles in such fluids.

Our work is limited to the formation of gas bubbles emitted by a single orifice. Although this process is not industrially used, it must be studied before considering the emission of bubbles through several orifices.

1.1 *Bubble formation*

Bubbles formation from single orifices can be divided into two categories: formation under constant pressure and under constant flow. The influence of chamber volume is closely related to that of the pressure difference ΔP, across the orifice. When the pressure drop across the orifice is large and the pressure variations occuring during the formation of bubbles are small compared to the total pressure drop, the gas flow rate does not change during bubble formation, and the bubbles are said to form under constant flow conditions.

Similarly if conditions are such that on the air-supply side of the orifice the pressure is maintained constant during bubble formation, as the bubble size increases the pressure inside it decreases resulting in a higher gas flow rate into the bubble.

The principal models of bubble formation have been proposed by Davidson & Schuler (1960) and by Kumar & Kuloor (1969, 1970).

These descriptions of bubble formation suggest that the growth of the bubble results in a radial expansion and in a vertical translation. The relative significance of these two stages is subject to the interaction of the forces on the bubble. We compare these proposed models of formation with the experimental observations.

The non-Newtonian behaviour of a fluid influences the liquid viscosity and varies the drag coefficient of the bubble in a non-Newtonian way.

1.2 *Drag coefficient of a sphere moving in a non-Newtonian liquid*

Any consideration of the flow of a fluid around a submerged object, or the movement of such an object through a fluid of infinite extent can be explained by using the equations of continuity and motion given by Bird *et al.* (1960).

Consider a pseudoplastic fluid, the rheological behaviour of which can be represented by Ostwald-Dé Waele or power law model:

$$\mathcal{P} = 2m[2 \operatorname{trace}(E^2)]^{n-1/2}E \qquad [1]$$

where $\mathcal{P}$ is the shear stress tensor, E the velocity gradient tensor, and m and n are the consistency coefficient and the fluid behaviour index in the power law model respectively.

Dimensional analysis of the equation of motion enables us to obtain the Reynolds number associated with a power law fluid:

$$Re' = \frac{\rho_L D^n U^{2-n}}{m} \qquad [2]$$

where ρ_L is the density of the liquid, D the diameter of the bubble and U the velocity of the bubble.

Most investigators have studied the creeping flow of spheres or bubbles in a non-Newtonian power law fluid, and have obtained an approximate solution for the calculation of the drag coefficient, C_D, which is given by

$$C_D = \frac{24X_n}{Re'}, \qquad [3]$$

where X_n is a parameter dependent on n.

We represent the results obtained for rigid spheres and for bubbles on figure 1, with the curve $X_n = f(n)$.

We observe that the results of Wasserman & Slattery (1964), Hirose & Moo Young (1969), Nakano & Tien (1968) are in agreement, but in contradiction with those of Fararoui & Kintner (1961); the correction factor X_n for the non-Newtonian behaviour varies in opposite directions. The solutions given by the former authors are more realistic, because in using the equations of motion and continuity applied to the sphere, they determine the drag force F_t by integration on the whole sphere,

$$F_t = \frac{1}{2} C_{D\rho L} U^2 A, \qquad [4]$$

where A is the frontal area of the bubble.

By using [3] and [4] we obtain

$$F_t = \frac{12\pi X_n m}{2^n} r^{2-n} U^n, \qquad [5]$$

where r is the radius of the bubble.

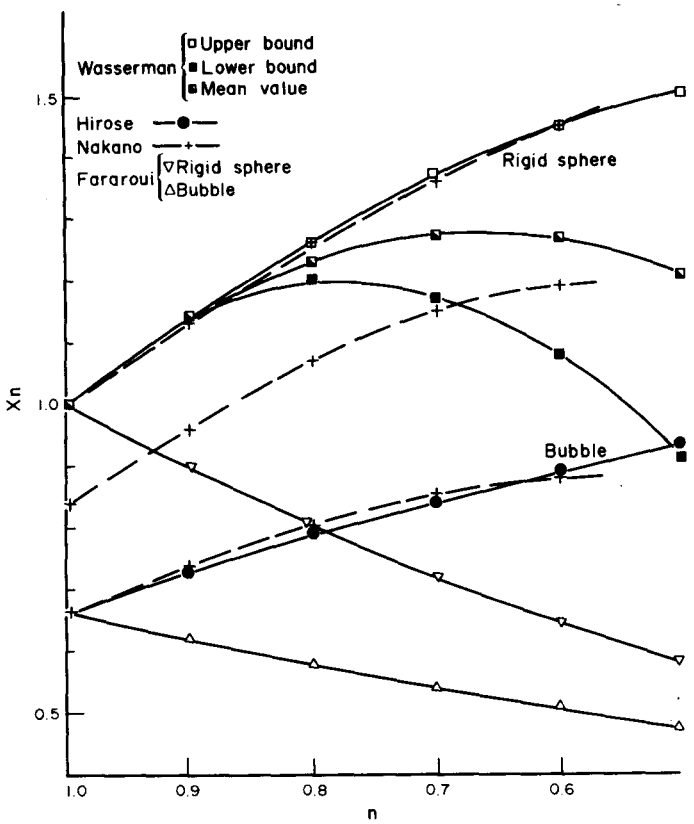

Figure 1. Theoretical correlations of X_n, from [3], with n for creeping flow of power law fluids around submerged spheres.

We can notice that when $n = 1$, $X_n = 1$, which is the case of a Newtonian fluid.

For pseudoplastic fluids, in the case of a rigid sphere, we take the mean of the upper and lower bounds of the X_n value which is given by Wasserman & Slattery (1964). In all cases, X_n is greater than one.

For bubbles, X_n is given by the results of Hirose & Moo Young (1969) or Nakano & Tien (1968).

1.3 *Motion of a gas bubble in a liquid*

The conditions of motion of a gas bubble in a liquid are determined by three factors, the Reynolds number, the bubble shape and the interface characteristics.

The only known theoretical solutions for non-Newtonian fluids are for power law liquids, and are presented by Astarita & Apuzzo (1965).

Stokes regime: a gas bubble moves in the Stokes regime when the liquid is in creeping flow, the bubble is spherical and the interface is rigid.

Hadamard regime: a gas bubble moves in the Hadamard regime when the liquid is in creeping flow, the bubble is spherical and the interface is free.

Garner & Hammerton (1954) have studied the movement inside rising bubbles in Newtonian liquids. For different experimental conditions, they have represented the ratio

$$\frac{\text{Velocity of rising bubble}}{\text{Velocity given by Stokes law}}$$ as a function of the Reynolds number, shown figure 2.

The transition from rigid to circulating conditions appears for a Reynolds number equal to 0.01. For a Reynolds number about $0.5 \sim 1$, the bubbles behave as rigid spheres (Stokes law).

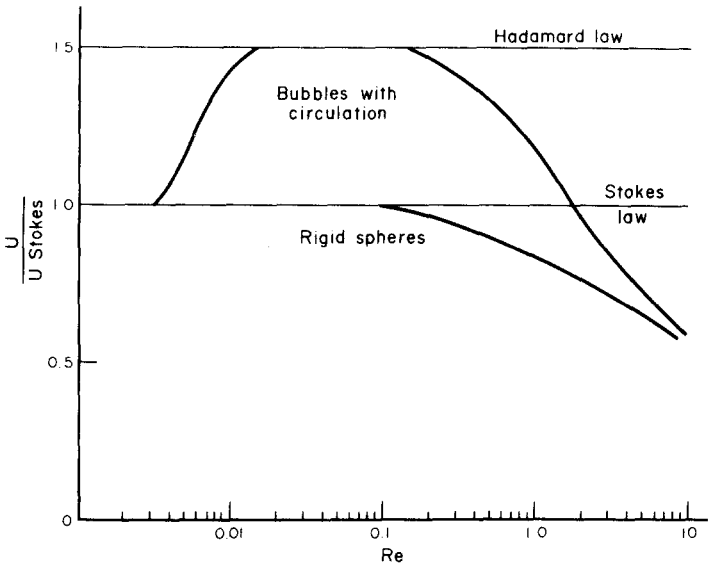

Figure 2. Divergence of the rate of rise of bubble from Stokes' law.

It will be obvious that for a non-Newtonian fluid, we will obtain the same curve as figure 2. In this case for a circulating bubble, the ratio U/U_{Stokes} will be greater than 1.5, and the fluid will have elastic properties.

2. EXPERIMENTAL STUDY

This experimental study has concentrated on bubble formation from single orifices in a pseudoplastic liquid.

2.1 *Experimental apparatus*

A schematic diagram of the apparatus is shown in figure 3. A rectangular Plexiglas tank of

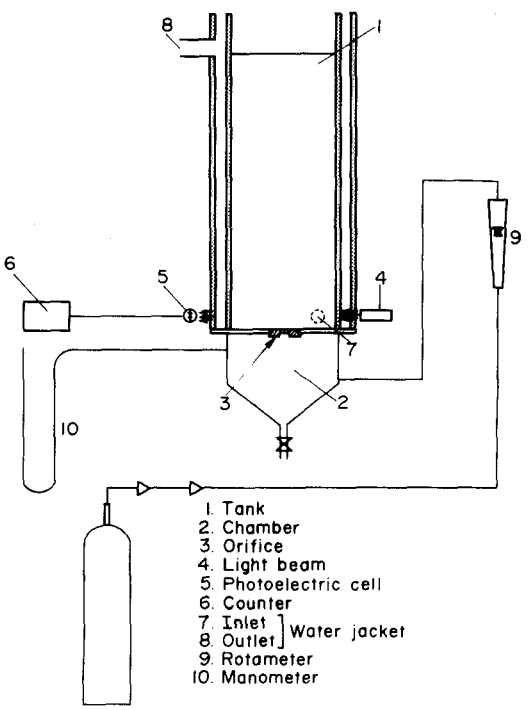

Figure 3. Schematic diagram of the apparatus used for the formation of bubbles.

dimensions $0.30 \times 0.30 \times 1.20$ m contained the liquid. A circulating water jacket, also constructed of Plexiglas was used to maintain the operating temperature at 25°C.

Nitrogen was supplied from a high pressure bottle and underwent a two stage expansion for its utilisation. The flow rate was adjusted and measured by a valve and a rotameter. To obtain a bubble emission at constant pressure, the gas entered a 30 l drum, from which it passed into the liquid through a stainless steel orifice. The pressure in the chamber below the orifice was measured by two manometers, mercury gauge and water manometer for low pressures.

The frequency of bubble formation was determined by a system including a luminous beam, a photoelectric cell, an electronic amplifier and a counter.

2.2 *Characteristics of the studied liquid*

We used an aqueous solution of sodium carboxymethyl cellulose (C.M.C.) at 3% in weight. The molecular weight of C.M.C. is about 400,000.

The rheological behavior of this solution is pseudoplastic.

The flow properties of C.M.C. solution have been determined by a concentric cylinder rotary viscosimeter. For a range of shear rates, from 5 to 200 s^{-1}, the parameters of the power law, m and n are determined to be

$$m = 3.04 \ (\text{kg.m}^{-1} \times \text{s}^{n-2});$$

$$n = 0.68;$$

$$a^2 = 1.$$

a^2 is the coefficient which measures the degree of perfection of the regression line where $a^2 = 1$ indicates ideal adjustment.

The rheological power law model of the 3% C.M.C. solution is

$$\tau = 3.04 E_0^{0.68} \qquad [6]$$

where τ is the shear stress and E_0 the shear rate.

With the degradation of the polymer solution and operational errors, the maximum deviation is below 6% for m and 3% for n. We have presented on figure 4 the rheogram: shear stress τ against shear rate E_0 and on figure 5 the apparent viscosity μ_a against shear rate of the C.M.C. solution:

$$\mu_a = \frac{\tau}{E_0} = m E_0^{n-1} \qquad [7]$$

Since n is less than unity for pseudoplastic fluids, [7] shows that the apparent viscosity decreases with increasing shear rate.

2.3 *Experimental procedure*

For a given flow rate, when the pressure in the chamber below the orifice is stabilised, we have measured the frequency of bubble formation during a long time (3 min). For several tests, the maximum deviation between these measurements is less than 2%.

We have used a camera, the objective of which was placed 50 cm from the orifice, with a speed of 100 images per sec. With this camera, we followed the bubble growth during its formation at the orifice. This work has been realised with the 3% C.M.C. solution, and with an orifice radius $R_o = 0.1265 \times 10^{-2}$ m.

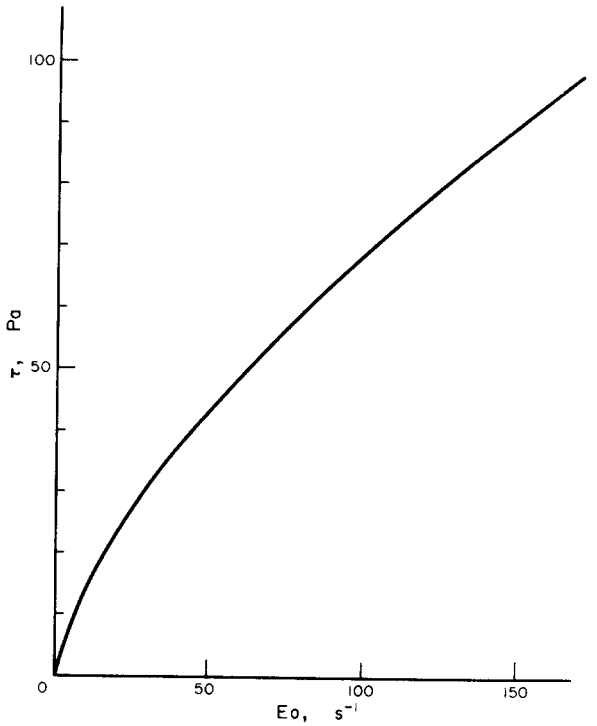

Figure 4. Flow curve for C.M.C. solution: $\tau = 3.04E_0^{0.68}$

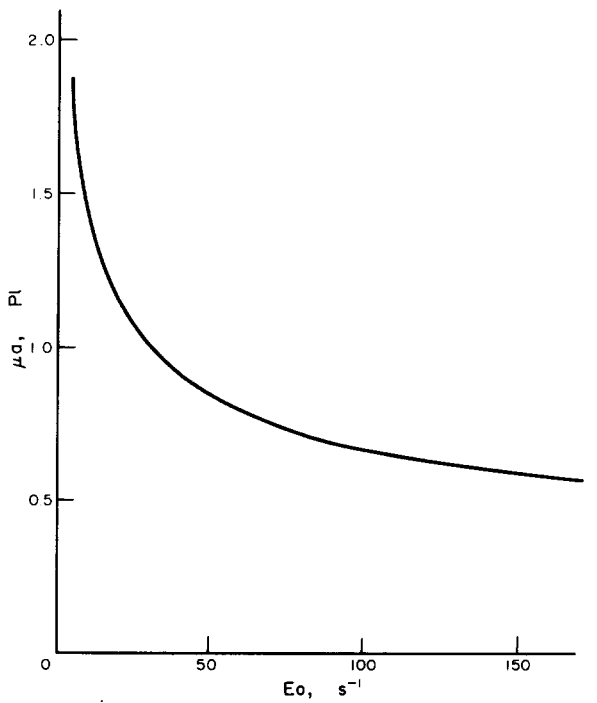

Figure 5. Variation of apparent viscosity, for C.M.C. solution: $\tau = 3.04E_0^{0.68}$ with shear rate.

The orifice constant C_ϕ has been obtained by measuring the orifice pressure drop ΔP, without liquid:

$$Q = C_\phi(\Delta P)^{1/2} \qquad [8]$$

where Q is the volumetric flow rate.

Equation [8] gives: $C_\phi = 4.537 \times 10^{-6}\ m^{7/2}/kg^{1/2}$ for the chosen orifice.

2.4 *Description of the experimental bubble formation*

2.4.1 *Qualitative analysis.* The cinephotographic observations enabled us to analyse the phenomenon with good precision.

We can distinguish three formation types:

1st *type*: Very low flow rates; the bubble begins to grow remaining spherical, its base is fixed to the orifice tip. The bubbles obtained are very small, and the frequency of formation is low. For greater bubble volumes, the bubble begins to draw out just before detachment.

This formation type corresponds to an orifice Reynolds number less than 1000.

2nd *type*: For higher flow rates, an ellipsoïdal bubble, with long vertical axis appears at the orifice, while a necking is formed at the bubble base. This necking is accentuated until the bubble breaks off.

3rd *type*: For orifice Reynolds numbers greater than 4000, bubbles are formed at the termination of a gaseous jet, rather than at the orifice tip.

According to the operating conditions, bubble coalescence occurs very close to the orifice and it is possible to form groups of two bubbles. It is to be noticed that the formation of two consecutive bubbles is different, and we observe that the volume of the second bubble is smaller than the volume of the first one.

These remarks lead us to believe that we cannot represent all the results by a single formation model.

For the first type of formation, the flow is a function of the extent to which the bubble has already been formed. The bubble is formed under constant pressure conditions.

For greater flows the bubble is formed at the termination of a gaseous jet. There therefore exists a point situated above the orifice tip, which acts as a gaseous source feeding the bubble. Under these conditions, we can consider that the flow rate is constant and cannot present a pulsing regime related to the frequency of bubble formation.

For intermediate flows of the second type, bubble formation takes place between the two limiting cases: formation under constant pressure and under constant flow conditions.

2.4.2 *Experimental results.* By the film analysis, we have determined the variations of bubble radius during the formation as a function of time.

For radius, we have used the radius equivalent to a sphere of equal volume, as calculated by l'Ecuyer & Murthy (1965).

We have presented the variation of the bubble radius as function of time on the curves (figures 6–9) for four experimental conditions (table 1).

We have also indicated in all cases the final bubble radius r_{exp} calculated from the experimental volume V_{exp} and the formation time of the bubble t_{exp}, from the frequency of formation N, so

$$r_{exp} = \left(\frac{3V_{exp}}{4\pi}\right)^{1/3}$$

and $t_{exp} = 1/N$.

It appeared that in all cases the volume-equivalent radius would give good agreement, since the data pass approximately through the point r_{exp}, t_{exp}, as shown on the figures. The formation

Table 1.

Tests	$10^6 Q(m^3/s)$	P_o(Pa)	Orifice Reynolds number	N (S^{-1})	$10^6 \times V$ (m^3)
A	20.5	10	688	4.17	4.92
B	29.75	10	999	5.86	5.07
C	61.5	98	2066	7.49	8.21
D	143	900	4800	10.28	13.91

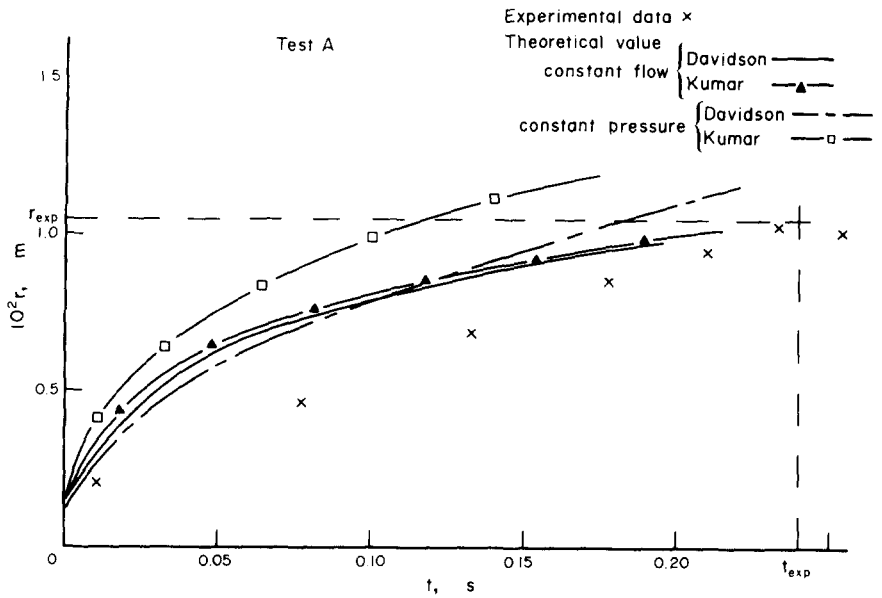

Figure 6. Comparison of theoretical and experimental bubble radius with time for A.

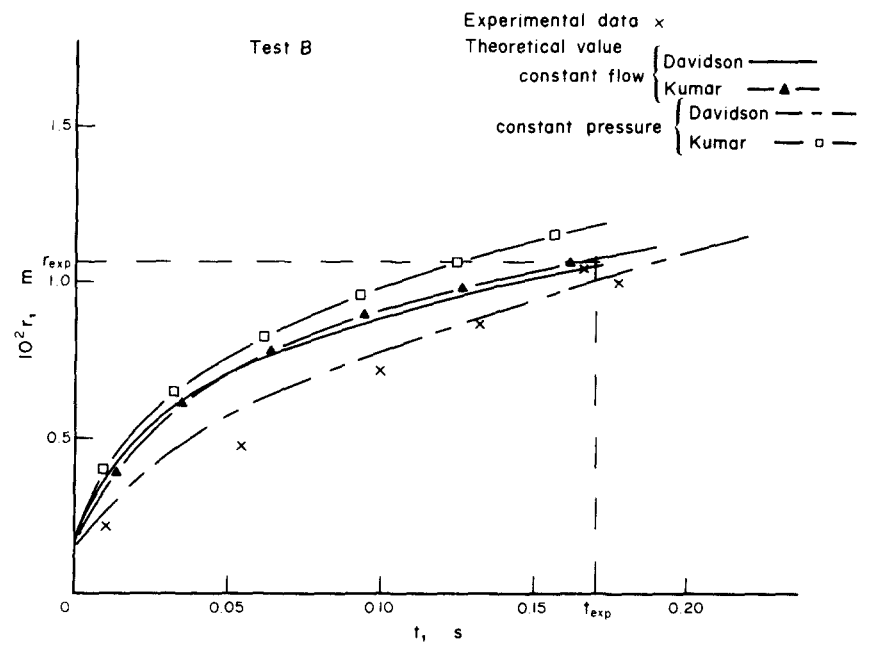

Figure 7. Comparison of theoretical and experimental bubble radius with time for B.

time calculated by the cinematographic method and the frequencies are in agreement. We notice that there is a reduction in bubble radius following detachment; this is due to some gas volume being left at the orifice after detachment.

3. *Theoretical modelling*

We shall now compare the experimental results with the formation models obtained by using the hypothesis proposed by Davidson & Schuler (1969) and by Kumar & Kuloor (1969, 1970) for the formation of bubbles in a pseudoplastic liquid.

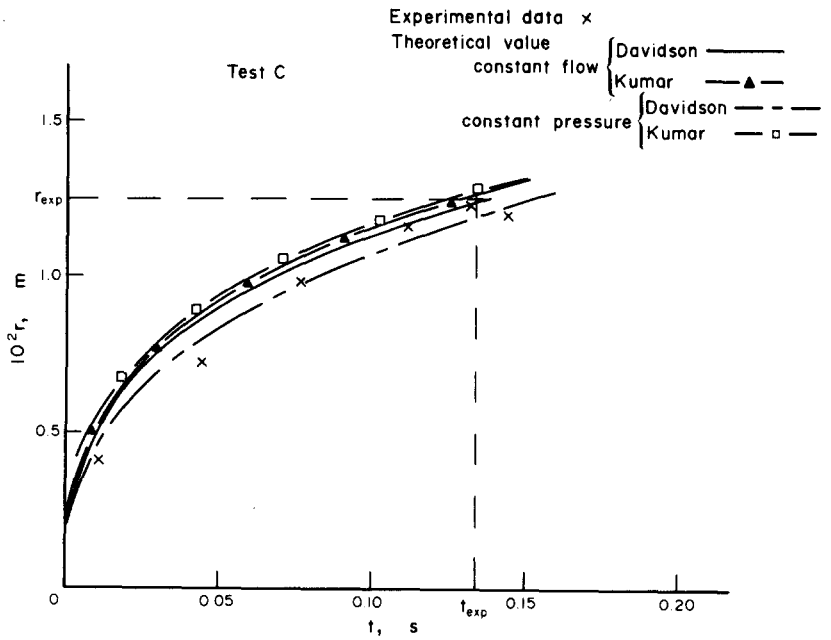

Figure 8. Comparison of theoretical and experimental bubble radius with time for C.

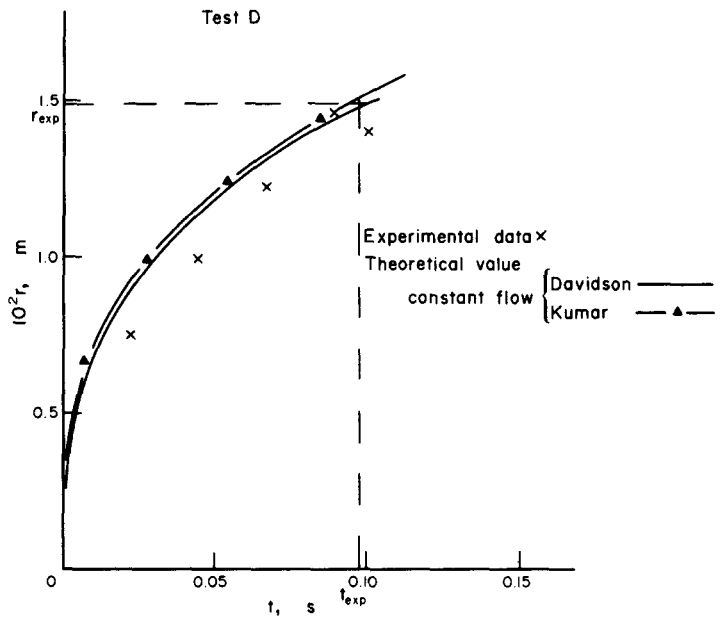

Figure 9. Comparison of theoretical and experimental bubble radius with time for D.

The forces operating during the bubble formation in a liquid are

a. Buoyancy:

$$F_A = V\rho_L g, \text{ if } \rho_G \ll \rho_L$$

where V is the bubble volume, ρ_G the density of the gas, and g the acceleration due to gravity.

This force is overestimated, because it does not take into account the junctions between the bubble and the orifice. The correction term is:

$$\frac{\pi_\phi^2}{4}(P_e - P_i)$$

where ϕ is the diameter of the orifice, P_e and P_i: the pressure outside and inside a bubble respectively. Therefore

$$F'_A = F_A - \frac{\pi\phi^2}{4}(P_e - P_i)$$

b. Surface tension:

$$F_\sigma = \pi\phi\sigma \cos\theta$$

where σ the surface tension and θ the contact angle.

c. Drag force: F_t

If we suppose, that during the formation, the bubble moves in creeping flow in a non-Newtonian power law fluid, the drag force is given by [5]

$$F_t = \frac{12\pi X_n m r^{2-n}}{2^n} U^n.$$

By application of Newton's second law, we obtain

$$F'_A - F_\sigma - F_t = \frac{\mathrm{d}(MU)}{\mathrm{d}t} \qquad [9]$$

M is the virtual mass of the bubble proposed by Milne-Thomson (1955),

$$M = \frac{11}{16}\rho_L V,$$

U is the rising velocity of the bubble,

$$U = \frac{\mathrm{d}r}{\mathrm{d}t} = \frac{Q}{\pi_D^2},$$

and Q is the flow rate:

$$Q = \frac{\mathrm{d}V}{\mathrm{d}t}.$$

The term $\mathrm{d}(MU)/\mathrm{d}t$ must be determined:

$$\frac{\mathrm{d}(MU)}{\mathrm{d}t} = M\frac{\mathrm{d}U}{\mathrm{d}t} + U\frac{\mathrm{d}M}{\mathrm{d}t}$$

with:

$$\frac{\mathrm{d}M}{\mathrm{d}t} = \frac{11}{16}\cdot\rho_L\cdot\frac{\mathrm{d}V}{\mathrm{d}t} = \frac{11}{16}\cdot\rho_L\cdot Q$$

and:

$$\frac{\mathrm{d}U}{\mathrm{d}t} = \frac{\mathrm{d}U}{\mathrm{d}D}\frac{\mathrm{d}D}{\mathrm{d}t} = \frac{-4Q^2}{\pi^2 D^5}$$

Thus,

$$\frac{\mathrm{d}(MU)}{\mathrm{d}t} = \frac{11}{16}\cdot\rho_L\cdot\frac{Q^2}{\pi D^2}\cdot\frac{1}{3}.$$

For our operating conditions we examine the importance of every term in order to make simplifications.

The term of surface tension force is always lower than 60×10^{-5} Newtons.

The over-evaluation of the buoyancy at the orifice level,

$$\frac{\pi\phi^2}{4}(P_i - P_e) = \frac{\pi\phi^2}{4} \cdot \frac{4\sigma}{2r}$$

is about 10×10^{-5} N.

For extreme conditions the buoyancy and the drag force can range from 1000×10^{-5} to 20000×10^{-5} N. In every case the term $d(MU)/dt$ is represented at most 5% of the buoyancy.

From this comparison, we have obtained the simplified relationship which only contains the buoyancy and drag forces.

$$V\rho_L g = \frac{12\pi X_n m r^{2-n}}{2^n} U^n. \qquad [10]$$

The cinematographic study enabled us to determine the bubble Reynolds number during the formation. The low Reynolds number values, 0.04–6, have shown that the bubble is moving in creeping flow. We shall suppose that the moving bubble obeys Stokes regime, (figure 2), i.e. it behaves like a solid sphere.

Under these conditions, the correction factor X_n is determined by taking the mean value of the upper and lower bounds which have been obtained by Wasserman & Slattery (1964).

We solve [10] using the assumptions of Davidson & Schuler (1960) or those of Kumar & Kuloor (1969, 1970) in the cases of bubble formation under constant flow rate and constant pressure conditions.

3.1 *Bubble formation models obtained by using the hypothesis of Davisson & Schuler* (1960)

The equation of upward motion is

$$V\rho_L g = \frac{12\pi X_n m}{2^n} r^{2-n} \left(\frac{ds}{dt}\right)^n. \qquad [11]$$

where s is the distance between the center of the bubble and the orifice.

The velocity of the center of the bubble is given by

$$\frac{ds}{dt} = \left(\frac{2^n \rho_L g r^{1+n}}{9 X_n m}\right)^{1/n} \qquad [12]$$

3.1.1. *Formation under constant pressure.* For each orifice considered, the gas flow rate is proportional to the square root of the pressure drop across the orifice,

$$Q = C_\phi \left(P_0 - \frac{2\sigma}{r} + \rho_L g s\right)^{1/2} = \frac{dV}{dt} \qquad [13]$$

where $P_0 = P_1 - \rho_L g h$, P_1 is the pressure in the chamber, and h is the orifice submergence.

The bubble is initially spherical and tangential to the orifice. The normal component of the surface tension is very small and its effect can thus be neglected. No doubt this is due to surface tension effects being less evident for highly viscous liquids, which is the case with this CMC solution.

The orifice equation becomes:

$$Q = C_\phi (P_o + \rho_L g s)^{1/2}. \quad [14]$$

Further:

$$Q = \frac{dV}{dt} = 4\pi r^2 \frac{dr}{dt}.$$

Thus:

$$\frac{dr}{dt} = \frac{C_\phi}{4\pi r^2}(P_0 + \rho_L g s)^{1/2}. \quad [15]$$

Equations [15] and [12] have been solved simultaneously for r, s, using a Runge–Kutta numerical technique for the initial conditions at $t = 0$, $r = R_o$ where R_o is the radius of the orifice, $s = 0$, $ds/dt = 0$.

The detachment criterion was taken when $s = r + R_o$.

3.1.2 *Formation under constant flow.* At any instant, the bubble volume is given by:

$$V = Qt = 4/3\pi r^3,$$

so

$$r = \left(\frac{3Qt}{4\pi}\right)^{1/3}.$$

Equation [12] becomes:

$$\frac{ds}{dt} = \left(\frac{2^n \rho_L g}{9 X_n m}\right)^{1/n} \left(\frac{3Q}{4\pi}\right)^{(1n/3n)} t^{(1+n/3n)}. \quad [16]$$

By integrating [16], we obtain the final equation:

$$V = \left(\frac{9 X_n m}{2^n \rho_L g}\right)^{3/1+3n} \left(\frac{4\pi}{3}\right)^{1/1+3n} \left(\frac{1+4n}{3}\right)^{3n/1+3n} Q^{3n/1+3n}. \quad [17]$$

Remark: In the case of a Newtonian liquid, with $n = 1$, $X_n = 1$ and $m = \mu$: the viscosity of the liquid, [17] becomes:

$$V = \left(\frac{15\mu Q}{2\rho_L g}\right)^{3/4} \left(\frac{4\pi}{3}\right)^{1/4}.$$

We have found the equation proposed by Alran (1971) and by Davidson & Schuler (1960) for the bubble formation in highly viscous liquids.

3.2 *Bubble formation models obtained by using the hypothesis of Kumar & Kuloor* (1969, 1970)

In this model, the bubble formation takes place in two stages, the expansion stage and the detachment stage. The bubble is assumed to stay at the orifice in the first stage, whereas in the second stage it is assumed to move upward from the tip until it detaches.

In neglecting the inertial and surface tension forces, the end of the first stage occurs when the upward buoyancy force is equal to the downward drag force,

$$F_A = F_t,$$

with

$$F_A = V_E \rho_L g,$$

$$F_t = \frac{12\pi X_n m}{2^n} r^{2-n} \left(\frac{dr}{dt}\right)^n$$

where V_E = volume of the force-balance bubble at the end of the first stage.

3.2.1 *Formation under constant pressure.* As with Davidson & Schuler's (1960) model the orifice equation is given by

$$\frac{dr}{dt} = \frac{C_\phi}{4\pi r^2}(P_0 + \rho_L g r)^{1/2}. \qquad [18]$$

Equation [18] is integrated numerically with the initial conditions that $t = 0$, $r = R_o$.

The integration is stopped when the force–balance bubble is obtained at the end of the first stage,

$$V_E \rho_L g = \frac{12\pi X_n m}{2^n} r^{(2-n)}\left(\frac{dr}{dt}\right)^n. \qquad [19]$$

We have obtained the formation time t_E, the bubble volume V_E, and the gas flow rate Q_E at the end of the first stage.

During the second stage, the gas flow rate can be assumed to be constant and equal to Q_E.

At any time, the motion equation is given by

$$F_A = F_t$$

with

$$V = V_E + Q_E \cdot t$$

and

$$F_t = \frac{12\pi X_n m}{2^n} r^{2-nu'/m}.$$

Here u', the velocity of the bubble center is made of two components: the velocity of the bubble base due to the movement and the velocity of the center due to the expansion. Thus

$$u' = u + \frac{dr}{dr},$$

where $u = dx/dt$, x = distance traversed by the base of the bubble.

We obtain:

$$u = \left(\frac{\rho_L g 2^n}{12\pi X_n m \left(\frac{3}{4\pi}\right)^{2-n/3}}\right)(V_E + Q_E t)^{1+n/3n} - \frac{Q_E}{\left(\frac{3}{4\pi}\right)^{2/3} \cdot 4\pi}(V_E + Q_E t)^{-2/3} \qquad [20]$$

Equation [20] is integrated with the conditions

$$\text{at } t = 0, \quad V = V_E, \quad x = 0$$

at $t = t_F$, $V = V_F$, $x = r_E$, r_E bubble radius at the end of the first stage.

We have thus obtained the final time, t_F, and the final volume, V_F, of the bubble formation.

3.2.2 *Formation under constant flow rate.* In this case the bubble volume is given by $V = Qt$. At the end of the first stage we have $F_A = F_t$. Thus,

$$V_E \rho_L g = \frac{12\pi X_n m}{2^n (4\pi)^n}\left(\frac{3}{4\pi}\right)^{2-3n/3} V_E^{2-3n/3} Q^n. \qquad [21]$$

Solving for V_E, we obtain:

$$V_E = \left(\frac{12\pi X_n m}{2^n(4\pi)^n \rho_L g}\right)^{3/1+3n} \left(\frac{3}{4\pi}\right)^{2-3n/1+3n} Q^{3n/1+3n}. \quad [22]$$

The second stage is identical to the formation under constant pressure condition.

2. DISCUSSION

We have compared the results obtained by these models with experimental data on figures 6–9.

First, we notice a small difference between the values calculated by the models using the hypotheses of Davidson & Schuler (1960) and those of Kumar & Kuloor (1969, 1970). During formation, the variation of the experimental bubble radius lie under theoretical values, because the assumption of spherical bubble is far from reality.

With the data in tables 2 and 3, the comparison between the theoretical and experimental final values of the bubble volume and formation time leads us to think that for an orifice Reynolds number greater than 1000 (tests B, C, D) the bubble formation can be represented by constant flow model. The bubble is comparable to a rigid sphere moving in the Stokes regime. In this case, Davidson & Schuler's model agrees better than Kumar & Kuloor's model.

For a Reynolds number lower than 1000, the formation under constant pressure appears more suitable. In these conditions, the Reynolds number of the bubble is very low, between 0.04 and 1.43. So, from figure 2, the behaviour of the bubble will be included between the two limit cases, Hadamard and Stokes' regimes. In table 4, we have compared the experimental results with theoretical values obtained with Davidson & Schuler's model for a bubble moving in

Table 2. Comparison with models obtained by using the hypotheses of Davidson & Schuler (1960) (Stokes law; $X_n = 1.27$)

			Constant gas flow rate				Constant pressure			
Test	$10^6 \times V_{exp}$ (m^3)	t_{exp} (s)	$10^6 \times V_{th}$ (m^3)	$\frac{V_{exp}}{V_{th}}$	t_{th} (s)	$\frac{t_{exp}}{t_{th}}$	$10^6 \times V_{th}$ (m^3)	$\frac{V_{exp}}{V_{th}}$	t_{th} (s)	$\frac{t_{exp}}{t_{th}}$
A	4.92	0.24	3.99	1.23	0.195	0.81	6.6	0.75	0.22	1.09
B	5.07	0.17	5.13	0.99	0.172	0.99	6.6	0.77	0.22	0.77
C	8.21	0.135	8.34	0.98	0.138	0.98	8.75	0.94	0.16	0.84
D	13.91	0.097	14.68	0.95	0.104	0.93	15.83	0.88	0.116	0.84

Table 3. Comparison with models obtained by using the hypotheses of Kumar & Kuloor (1969, 1970) (Stokes law: $X_n = 1.27$)

			Constant gas flow rate				Constant pressure			
Tests	$10^6 \times V_{exp}$ (m^3)	t_{exp} (s)	$10^6 \times V_{th}$ (m^3)	$\frac{V_{exp}}{V_{th}}$	t_{th} (s)	$\frac{t_{exp}}{t_{th}}$	$10^6 \times V_{th}$ (m^3)	$\frac{V_{exp}}{V_{th}}$	t_{th} (s)	$\frac{t_{exp}}{t_{th}}$
A	4.92	0.24	4.38	1.12	0.213	1.13	7.15	0.69	0.173	1.39
B	5.07	0.17	5.62	0.90	0.189	0.90	7.15	0.71	0.173	0.98
C	8.21	0.135	9.15	0.90	0.149	0.91	9.16	0.90	0.150	0.90
D	13.91	0.097	16.12	0.86	0.112	0.87	16.07	0.87	0.115	0.84

Table 4.

		constant pressure Davidson & Schuler's model ($X_n = 0.84$, Hadamard Law)	
Test	$10^6 \times V_{exp}$ (m^3)	$10^6 \times V_{th}$ (m^3)	$\frac{V_{exp}}{V_{th}}$
A	4.92	4.41	0.90

the Hadamard regime. Thus depending upon experimental conditions, the interface of a gas bubble will tend to reach one or the other of the two extreme cases: free interface or rigid interface.

For generalisation, we have considered the change in volume of the bubbles as a function of the gas flow on figure 10 for the same orifice. This curve can be considered to consist in two zones:

(a) At low flow rates, the volume of the bubble is almost constant or increases only slightly. The bubbles are small and clearly separated. In this zone, the effect of pressure on the frequency of bubble generation is significant.

The orifice Reynolds number is less than or close to 1000, and it can be considered that the bubble formation takes place at constant pressure.

(b) At high flow rates, the bubble volume increases steadily because the frequency of formation is almost constant. It is considered that bubble formation takes place at almost constant flow rate.

The orifice Reynolds number is greater than 1000. Under some conditions, it has been observed that the bubbles coalesce at the orifice.

Since the way in which double bubbles form is different from that of single bubbles, for the rest of the investigation only results obtained without coalescence will be considered.

For high flow rates, the straight line calculated by the constant gas flow rate models obtained by using the hypothesis of Davidson & Schuler (1960) [17] and those of Kumar & Kuloor (1969, 1970) has been marked on figure 10; with the assumption that the motion of the bubble conforms with Stokes law.

It can be seen that the experimental results agree well with the theoretical curve of Davidson & Schuler's model, but the formation of bubbles cannot be represented by a unique relationship. According to the experimental conditions, the constant gas flow rate model cannot represent the formation of bubbles at low flow rate.

So, for studying bubble formation at constant pressure, we have considered the variation in bubble volume at the orifice as a function of pressure drop P_0 in figure 11. The theoretical curves obtained by using the constant pressure models of Davidson & Schuler and Kumar & Kuloor have been marked on figure 11.

As we have seen before for this viscous solution of CMC, the experimental points lie between the curves corresponding to Stokes' law and those corresponding to Hadamard's conditions.

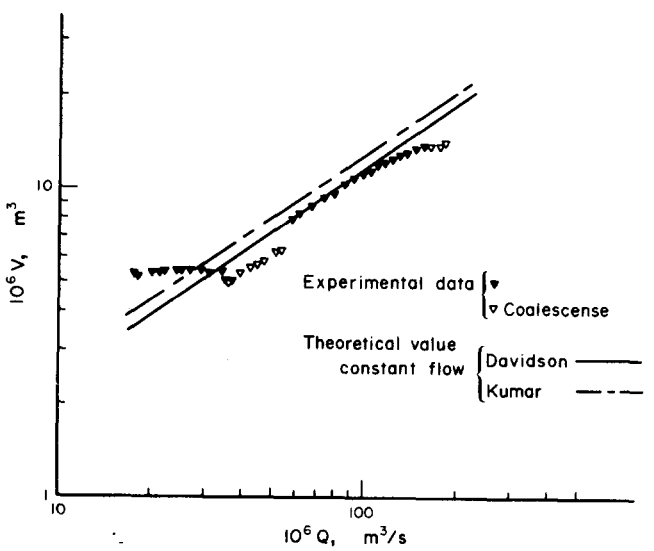

Figure 10. Variation of bubble volume with gas flow rate for solution 3% C.M.C., and orifice radius: $R_0 = 0.1265 \times 10^{-2}$ m.

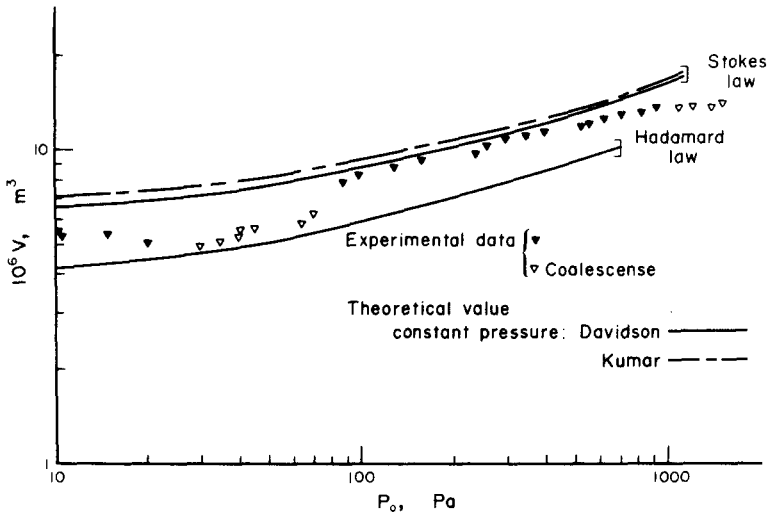

Figure 11. Variation of bubble volume with orifice pressure drop for solution 3% C.M.C., and orifice radius: $R_0 = 0.1265 \times 10^{-2}$ m.

5. CONCLUSION

The formation of gas bubbles in a highly viscous non-Newtonian pseudoplastic liquid was studied theoretically and experimentally.

We have seen that under experimental conditions the formation of bubbles conformed approximately with either the constant pressure or constant gas flow rate models obtained by using the hypotheses of Davidson & Schuler, and those of Kumar & Kuloor.

When the orifice Reynolds number is lower than 1000, bubbles are formed under constant pressure conditions; for an orifice Reynolds number higher than 1000, the bubbles are formed under constant flow rate conditions.

The comparison of theoretical variation of bubble radius seems to show that Davidson & Schuler's and Kumar & Kuloor's are in agreement, but Davidson & Schuler's model is more suitable than Kumar & Kuloor's model for representing bubbles formation.

REFERENCES

ALRAN, C. 1971 Thèse de Doctorat ès Sciences Physiques, Paul-Sabatier, Toulouse.

ASTARITA, G. & APUZZO, G. 1965 Motion of gas bubbles in non-Newtonian liquid. *A.I.Ch.E.Jl.* **11**, 815–820.

BIRD, R. B., STEWART, W. E. & LIGHTFOOT, E. N. 1960 *Transport Phenomena.* Wiley, New York.

DAVIDSON, J. F. & SCHULER, B. O. G. 1960 Bubble formation at an orifice in a viscous liquid. *Trans. Inst. Chem. Engrs* **58**, 144–156.

FARAROUI, A. & KINTER, R. C. 1961 Flow and shape of drops in non-Newtonian fluids. *Trans. Soc. Rheol.* **5**, 369–380.

GARNER, F. H. & HAMMERTON, D. 1954 Circulation inside gas bubbles. *Chem. Engng Sci.* **3**, 1–11.

HIROSE, T. & MOO YOUNG, M. 1969 Bubble drag and mass transfer in non-Newtonian fluids: creeping flow with power-law fluids. *Can. J. Chem. Engng* **47**, 265–267.

KUMAR, R. & KULOOR, N. R. 1969 Bubble formation in viscous liquids under constant flow conditions. *Can. J. Chem. Engng* **48**, 383–388.

KUMAR, R. & KULOUR, N. R. 1970 The formation of bubbles and drops. *Adv. Chem. Engng* **8**, 255–368.

l'ECYER, M. R. & MURTHY, S. N. B. 1965 Energy transfer from a liquid to gas bubbles forming at a submerged orifice. NASA TND 2547.

MILNE-THOMPSON, L. N. 1955 *Theoretical Hydrodynamics*. 3rd Ed. Macmillan, London.

NAKANO, Y. & TIEN, C. 1968 Creeping flow of power law fluid over Newtonian fluid sphere. *A.I.Ch.E.Jl.* **14**, 145–151.

WASSERMAN, M. L. & SLATTERY, J. C. 1964 Upper and lower bounds on the drag coefficient of a sphere in a power-model fluid. *A.I.Ch.E.Jl.* **10**, 383–388.